GENERAL ATOMIC

GA-A14324

RESIDUAL STRESS AND STRAIN EXAMINATION IN PEACH BOTTOM FUEL TEST ELEMENTS

by
C. F. WALLROTH, C. M. MILLER, and J. J. SAURWEIN

MAY 20, 1977

DISCLAIMER

GENERAL ATOMIC

GA-A14324

RESIDUAL STRESS AND STRAIN EXAMINATION IN PEACH BOTTOM FUEL TEST ELEMENTS

by
C. F. WALLROTH, C. M. MILLER, and J. J. SAURWEIN

This is a preprint of a paper to be presented at the ANS Topical Meeting, 4th International Conference on Structural Mechanics in Reactor Technology, August 15, 1977, San Francisco, California and to be published in the Proceedings.

Work supported in part under
Contract EY-76-C-03-0167
Project Agreement No. 17
for the San Francisco Operations Office
U.S. Energy Research and Development Administration

GENERAL ATOMIC PROJECT 3224

MAY 20, 1977

ABSTRACT

An examination of residual stresses and strains has been carried out experimentally on structural graphite components removed from Peach Bottom High-Temperature Gas-Cooled Reactor (HTGR) fuel elements. The purpose of this work is to confirm predicted stress distributions.

Twenty-nine teledial fuel elements (of six- and eight-hole design) were irradiated in the Peach Bottom HTGR to fluences of $\leq 4 \times 10^{25}$ n/m^2 ($E > 29$ fJ) and time-average temperatures up to 1100°C. The irradiation history was modeled with HTGR design codes. Performance predictions were verified by in-pile thermocouples and fuel burnup measurements. The predicted irradiation-induced strains were found to be in quantitative agreement with postirradiation measurements ($\leq$0.5% shrinkage over a 70-mm diameter). As a result of the temperature distribution in the teledial bodies, compressive stresses were predicted at the periphery and tensile stresses in the inner zones. A total of 19 graphite bodies from 8 different fuel elements were examined destructively for structural integrity and residual stresses. For the higher exposure elements, local stresses at shutdown in excess of the uniaxial strength of the material were predicted, yet no structural damage was found. This may be because uniaxial failure criteria are conservative. Axial strips of 460-mm length were cut and measured for changes in curvature, which indicate release of residual axial stresses. Release of compressive residual stresses was observed from slight extension of the strips when compared with length measurements before cutting.

Slices of 20-mm thickness were cut across the diameter of some teledial graphite bodies. Residual in-plane strain was released by a single radial cut from the outer surface to an uncooled center hole. The distance between grooves on either side of the cut was measured, as well

as the outside diameter change. The resulting mean contractions were 0.20 and 0.04 mm, respectively, and these can be interpreted in terms of material strain.

Primary loading tests were performed by hydraulic pressurization of fuel holes in the location of predicted peak secondary residual stresses. Standard radial compression tests were carried out for some of the slices.

A control program is being executed on unirradiated specimens. First indications from burst tests are that the net difference in strength of the graphite during irradiation is positive; i.e., the irradiation-induced stresses are generally exceeded by the strength increase of the material. Cases with decreases in the strength margin were also found.

The data from the tests have been statistically reduced. (176 strip, 93 radial compression, and 938 pressure burst examinations have been carried out on irradiated material.) These data will serve as a data bank for stress code verification and for the development of improved failure criteria for graphite. The structural soundness of the prismatic-type HTGR fuel element has again been proven and the measurability of axial and radial residual stresses in irradiated HTGR graphite has been demonstrated.

1. INTRODUCTION

An experimental program has been carried out to determine residual stresses and strains in structural graphite removed from fuel test elements irradiated in the Peach Bottom High-Temperature Gas-Cooled Reactor (HTGR). The purpose of this work is the confirmation of predicted stress distributions. The feasibility of destructive stress examination was demonstrated earlier by the Dragon Project [1] and by CEA, Saclay [2]. The status of the experimental results is presented here, and the correlations of experimental results with predictions are reported in a companion paper by Homeyer et al. [3].

The fuel test elements each contained three teledial graphite fuel bodies of 790 mm length and 70 mm outer diameter within a graphite sleeve. Each element was helium cooled from the outside. Design and performance details are reported by Turner et al. [4] and in Refs. 5 through 8. Figure 1 shows the cross sections of the eight- and six-hole teledial bodies, which were machined from H-327 graphite, a coarse-grain needle-coke graphite manufactured by Great Lakes Carbon Corporation (GLCC).

A total of 19 teledial fuel bodies from 8 fuel test elements were destructively examined. Slices of 20-mm thickness were cut and submitted to hydraulic burst, radial compression, and radial ring cut tests. Other fuel body sections were cut axially, yielding 457-mm-long strips of two designs, i.e., a thin strip along the fuel holes and a thick pie-shaped strip between fuel holes as shown in Fig. 1. A control program was carried out on unirradiated material, using the same test equipment for calibration and characterization purposes.

2. IRRADIATION AND STRESS HISTORY

Thirty-three fuel test elements were irradiated in the Peach Bottom HTGR to fast fluences of $\leq 4 \times 10^{25}$ n/m^2 (E > 29 fJ) and time-averaged graphite temperatures up to 1100°C. The irradiation conditions of the

eight teledial elements presently included in the destructive stress examination program are summarized in Table I. Data are given on a fuel body basis and are time and volume weighted averages. This information was obtained through computer simulation of the Peach Bottom reactor history with HTGR design codes. The temperature and fluence parameters "peak," "mean," "RMS_a," and "RMS_t" were selected to describe the irradiation conditions over the lifetime of each experiment. The peak fluence is the highest fluence level within the fuel body, and the peak temperature is the highest predicted graphite temperature during irradiation within the body (i.e., at the uncooled inner periphery). The root mean square RMS_a describes the variation along the length of the fuel body. RMS_t is the temporal variability of the temperatures. Any random errors originating from uncertainties in the predictions are in addition.

The experiments were monitored with thermocouples, and in-pile tungsten-rhenium thermocouple readings were corrected through recalibration after irradiation [6]. Absolute power and relative power profiles were measured via multiplex burnup determinations and fuel gamma scanning as described in Ref. 7. Agreement with predictions was found to be within ±10%. Predicted and measured temperature averages agreed within ±80°C and were usually in accord with power deviations.

The stress history of the experiment was simulated for a symmetrical unit cell with a finite element code GTEPC [9], a computer program for two-dimensional viscoelastic analysis of graphite. For the higher exposure elements, local stresses at shutdown in excess (by a factor of ≤ 1.5) of the uniaxial strength of the material were predicted, yet no structural damage was found. This may be because tensile failure criteria are conservative.

Due to azimuthal fuel loading variations, which originated from different thorium loadings and consequently different U-233 conversions, bow of the fuel bodies was observed which exceeded up to fivefold the nominal clearance between the graphite body and surrounding sleeve [8].

This resulted in an additional stress field with a maximum stress-to-strength ratio of 0.4, which has to be superimposed onto the symmetrical stress field.

3. FUEL BODY STRAIN

Diametrical strain was predicted and measured for several graphite fuel bodies. Predictions were based on unrestrained graphite dimensional change data obtained from isothermal and isoflux irradiation tests by Price and Beavan [10]. A comparison is given in Fig. 2 for twelve fuel bodies from four similar fuel test elements with a wide range of irradiation exposure (see Table I). Measurements are shown with 95% confidence estimates and agree quantitatively with the predicted strain of <0.5% shrinkage. Some qualitative differences can be recognized at the interface between fuel bodies. This results from a simplification in the thermal analysis which does not presently account for axial heat conduction. Other irregularities can be attributed to local power peaking originating from fuel inhomogeneities in the teledial fuel rods and from additional fuel located in center spine samples, as revealed from fuel gamma scanning [8]. Two of the low-temperature fuel bodies (bottom bodies in FTE-4 and FTE-6) show inversion in the measured strain toward the cooler end (left side in Fig. 2), which is not predicted. The good qualitative and quantitative agreement for the top body in FTE-5 is related to improved axial and radial heat transfer originating from in situ curing of the fuel rods (cure-in-place process), whereas all the other fuel bodies were loaded with loose rods after curing in packed alumina beds.

4. STRIP CUTTING

Table II summarizes the strip cutting results from 162 out of 196 irradiated strips taken from 12 fuel bodies. A typical bow line for one thick strip and two adjacent small strips is shown in Fig. 3. The concave side of these strips was pointing toward the center of the fuel element and the resulting maximum bow (arc-to-chord displacement) was defined

as positive bow. This is the expected direction of residual bow because the irradiation-induced shrinkage is larger at the hotter fiber for the tested graphite. Results were averaged for adjacent strips taken from the same fuel body. The amount of azimuthal variation can be recognized from the RMS variation given in Table II. With increasing fast fluence, the bow of the thin strips becomes smaller and even negative. Thick strips follow the same trend but with less negative bow. The graphite body of FTE-5 with overall highest exposure shows inversion of bow for nearly all strips. No structural damage was found except for some breakage of strips caused by the saw during cutting.

A significantly lower thermal expansivity at the hotter fiber than at the cooler one would explain the observed bow inversion. Therefore, a sensitivity experiment was carried out on five inversely bowed thin strips. One end was cantilevered inside a horizontal furnace, and the deflection of the free end of the strip was photographically recorded through a glass window during heatup to 1000°C and subsequent cooldown. The change in deflection was always away from the center of the fuel; i.e., the inversed bow increased further during heatup.

These changes in deflection are interpreted as being caused by differences in thermal expansivity between inner and outer fibers. The contribution to thermal stresses from differential expansivity was found to be approximately equal to that from the temperature gradient along the cross section of the strip. The experiment showed unambiguously a higher thermal strain at the inner fiber for all five strips tested. Thermal expansivity was ruled out as the possible cause for the inversion in bow. Measurement of the mean expansivity is planned on strip sections to establish the amount of thermal stresses after shutdown from measured properties. Knowing the residual stresses from bow and elongation measurements, the operational stresses at the end of irradiation can be determined by subtraction.

Large elongations were found for the thin and thick strips, which imply large compressive stresses on the order of -14 MPa. The uncertainty is high with ±40% which originates from the differential nature of the measured effect. Maximum residual bow measurements were more accurate because of the larger magnitude of the measured effect. The uncertainty was usually better than ±10%. The measured elongation was larger than predicted, whereas smaller than expected bow was found for the cases where the predicted direction of bow agreed with the observation [3].

The high compressive stresses have to be offset by very high tensile stresses in the one remaining inner section, which could not be measured. This raises the question of artificial elongation and bow of the strips during the cutting operation. First results on unirradiated strips show some residual bow in a random manner, which is inconclusive with regard to perturbations originating from the saw.

5. RING CUT, PRESSURE BURST, AND RADIAL COMPRESSION TESTS

Experimental results are presented in Table III and Figs. 4 through 7. Irradiation temperatures are referenced, which are predicted time averages for the location of crack initiation. Eight-hole slices failed under primary load (burst pressure and radial compression) at the inner fuel hole surface, while six-hole slices failed at the outer fuel hole boundary. The RMS variation for all observations and the fluence variation between test samples taken from the same fuel body are included in the figures.

A control program was carried out on several graphite bodies machined from the same graphite log. No significant difference in bursting pressure was found for the six- and eight-hole configurations, which is coincidental. Axial and azimuthal variations of the burst testing results correlate with tensile strength measurements made on surrounding graphite material.

Three eight-hole teledial bodies and four six-hole teledial bodies were manufactured from the same graphite log and have been correlated with fluence exposure. Usually, the irradiation temperature increased slightly with increased fluence because of decreases in thermal conductivity. Spreads in the observed results are associated with axial and radial variations within logs. In some cases, variations in connection with the bursting sequence were also observed; i.e., the burst pressure decreased with increasing numbers of bursted holes because of a possible weakening effect on the structure.

In-plane strain measurements are presented in Figs. 5 and 7 for the two measurement techniques applied, i.e., groove distance change and outer diameter change. Both methods correlate well with an approximate correlation factor of 5. This supports the reliability of the measurements. The ring closure is a result of residual hoop stresses, and mean contractions of 0.20 and 0.04 mm for groove change and diameter change, respectively, were found, which can be interpreted in terms of material strain. The eight-hole teledial results show a minimum at a fast fluence of 1.3×10^{25} n/m^2, which can be a material variation effect. The overall tendency for the two teledial configurations is an increase of ring closure with fluence, indicating increase of in-plane stresses with irradiation.

The primary load test results are shown in Figs. 4 and 6. Failure load and burst pressure increase with fluence for both teledial geometries. This means that the net effect between strength increase of the material and buildup of residual in-plane stresses is positive and that the safety margin of a graphite fuel element increases with exposure.

6. CONCLUSIONS

Destructive stress examinations have been done on a large number of graphite samples taken from a group of similar fuel test elements from

the Peach Bottom HTGR. The following conclusions can be drawn:

1. Diametrical fuel body strain was found to be in quantitative agreement with predictions.

2. Large stress levels in excess of the material strength were predicted during irradiation but no structural damage was found, which indicates conservatism in stress calculations.

3. Large elongations were observed for strips cut from the graphite bodies, which implies large compressive loads on the order of -14 MPa.

4. Very high tensile stresses would occur in a small inner section to balance the measured compressive stresses. A related question is possible artificial elongation and bow of the strips during the cutting operation. First control tests are inconclusive.

5. Residual bow measurements showed smaller bow than expected in the predicted direction (concave bow toward the center of the element) and bow in the opposite direction to that predicted for some elements.

6. Bow inversion was found to increase with higher fluences for thin strips. Bow inversion was also found for thick strips at the highest fluence level of 3.6×10^{25} n/m^2.

7. Differences in thermal expansivity were ruled out as a cause of the bow inversion. Differential expansivity was quantitatively determined via heatup of inversely bowed strips. The associated thermal strain was found to be equal to the thermal strain caused by temperature gradients. Through thermal expansivity measurements the thermal stresses after shutdown

can be determined, which lead via the measured residual stresses to the operational stresses based on property measurements independent of predictions.

8. Burst pressure tests on unirradiated control samples were found to correlate with tensile strength measurements made on surrounding graphite material. Burst tests should also give a strength distribution in irradiated material.

9. Ring closure measurements done by two different methods were found to correlate with each other and showed release of residual hoop stresses in the predicted direction. In-plane stresses increased with fluence.

10. Failure load and burst pressure were found to increase with irradiation exposure, which means a net increase in material strength over the in-plane stresses for the tested fluence range.

11. The good response found for residual bow, thermal strain, axial elongation, in-plane strain, and strength margin measurements allows the conclusion that the complex stress fields in irradiated graphite are measurable. These data should serve as a valuable data bank for stress code verification and material property change predictions and should help in improving failure criteria for graphite.

REFERENCES

[1]. Kinkead, A. N., P. Barr, and M. R. Everett, "The Thermal and Mechanical Performance of HTR Fuel Elements," Dragon Project Report DPR/847, September 1973.

[2]. Tortel, J., and G. Jouquet, CEA, Grenoble, private communication, March 1976.

[3]. Homeyer, W. G., F. K. Tzung, and D. D. Chiang, "Residual Stress in Peach Bottom Test Elements - Analysis vs. Experiment," same conference.

[4]. Turner, R. F., R. D. Burnette, and W. J. Scheffel, "HTGR Fuel Performance in the Peach Bottom Reactor," Gulf General Atomic Report Gulf-GA-A12675, July 9, 1973.

[5]. Wallroth, C. F., N. L. Baldwin, C. B. Scott, and L. R. Zumwalt, "Postirradiation Examination of Peach Bottom Fuel Test Element FTE-3," ERDA Report GA-A13004, General Atomic Company, August 15, 1975.

[6]. Wallroth, C. F., F. McCord, R. J. Mayer, and J. J. Saurwein, "Postirradiation Examination and Evaluation of Peach Bottom Fuel Test Element FTE-18," General Atomic Report GA-13699, June 1, 1976.

[7]. Wallroth, C. F., J. F. Holzgraf, D. D. Jensen, and L. R. Zumwalt, "Postirradiation Examination and Evaluation of Peach Bottom Fuel Test Element FTE-4," ERDA Report GA-A13452, General Atomic Company, to be published.

[8]. Wallroth, C. F., J. F. Holzgraf, and D. D. Jensen, "Postirradiation Examination and Evaluation of Peach Bottom Fuel Test Element FTE-6," ERDA Report GA-A13943, General Atomic Company, to be published.

[9]. Tzung, F. K., "GTEPC-2D, a Computer Program for Two-Dimensional Graphite Thermal-Elastic-Plastic-Creep Analysis, User's Manual," General Atomic Report GA-A13532, January 31, 1976.

[10]. Price, R. J., and L. A. Beavan, "Final Report on Graphite Irradiation Test OG-3," ERDA Report GA-A14211, General Atomic Company, January 1977.

TABLE I SUMMARY OF PEACH BOTTOM FUEL TEST ELEMENT IRRADIATION CONDITIONS

Fuel Element	Fuel Body	Graphite Temperature (°C)				Fast Fluence (10^{25} n/m^2)		
		Body Average	$\pm RMS_t$	$\pm RMS_a$	Body Max.	Body Average	$\pm RMS_a$	±Body Max.
FTE-1	1	794	ND	130	1153	.84	.24	1.12
	2	1036	21	36	1355	1.11	.05	1.16
	3	998	ND	36	1269	.66	.19	.92
FTE-2	1	736	ND	115	1120	1.27	.37	1.71
	2	950	ND	32	1234	1.70	.07	1.77
	3	912	ND	36	1180	1.03	.29	1.42
FTE-3	1	703	52	113	992	.41	.12	.55
	2	890	71	28	1145	.54	.02	.57
	3	860	62	33	1093	.34	.10	.48
FTE-4	1	743	28	122	1133	1.40	.40	1.88
	2	970	30	38	1237	1.94	.05	1.98
	3	955	34	44	1217	1.26	.35	1.72
FTE-5	1	742	ND	119	1166	2.73	.74	3.59
	2	953	80	34	1255	3.67	.07	3.74
	3	943	62	43	1207	2.58	.70	3.44
FTE-6	1	769	60	120	1181	2.10	.57	2.76
	2	998	90	41	1363	2.83	.05	2.88
	3	998	93	48	1405	1.98	.54	2.65
FTE-14	1	728	73	106	1085	.96	.26	1.27
	2	1013	90	64	1367	1.30	.03	1.33
	3	1042	103	47	1312	.89	.25	1.20
FTE-15	1	798	85	126	1287	1.49	.40	1.96
	2	1081	117	66	1528	2.02	.03	2.05
	3	1051	105	47	1383	1.46	.38	1.92

All data are preliminary.

RMS_t = temporal variability

RMS_a = axial variability

TABLE II SUMMARY OF RESIDUAL BOW AND ELONGATION MEASUREMENTS FOR 457 mm STRIPS CUT FROM PEACH BOTTOM HTGR FUEL TEST ELEMENTS

QUANTITY		DIMENSION	CONTROL PROGRAM 6 HOLE	CONTROL PROGRAM 8 HOLE	FTE-2 Body 2	FTE-3 Body 2	FTE-4 Body 2	FTE-5 Body 2	FTE-5 Body 3	FTE-6 Body 1	FTE-6 Body 2	FTE-6 Body 3	FTE-14 Body 2	FTE-15 Body 1	FTE-15 Body 2	FTE-15 Body 3
Fast Fluence (E>29fJ)		(10^{25}n/m^2)	NA	NA	1.69	0.52	1.87	3.63	2.40	2.34	2.79	1.80	1.29	1.78	2.05	1.18
Irradiation Temperature																
Thin Strip	Mean	(C)	NA	NA	ND	854	929	909	900	774	955	942	965	766	1013	1000
Thin Strip	ΔT	(C)	NA	NA		24	35	36	23	38	39	25	14	21	18	9
Thick Strip	Mean	(C)	NA	NA		934	1026	1009	966	869	1057	1010	1074	889	1134	1069
Thick Strip	ΔT	(C)	NA	NA		183	230	235	155	227	244	162	230	267	259	148
THIN STRIP																
Max.Residual Bow	Sample Size	(-)	3	4	6	8	8	6	7	8	7	8	5	6	5	5
	Mean	(mm)	.0	+.12	+.92	+.58	-.16	-2.57	+.02	+.20	-1.26	-.84	-1.50	+.56	-2.19	-2.82
	±RMS	(mm)	.37	.16	.20	.23	.71	.75	.35	.23	.38	.24	.41	.18	.35	.42
Elongation	Sample Size	(-)	ND	ND	6	8	8	ND	ND	ND	ND	ND	5	6	5	5
	Mean	(mm)			+.28	+.29	+.72						+.32	+.31	+.31	+.27
	± RMS	(mm)			.18	.10	.63						.05	.09	.05	.05
THICK STRIP																
Max.Residual Bow	Sample Size	(-)	ND	ND	4	8	8	8	8	8	8	8	6	6	5	6
	Mean	(mm)			+1.05	+.84	+.67	-.76	+.29	+.74	+.37	+.20	+.71	+.58	+.59	+.33
	±RMS	(mm)			.09	.06	.28	.60	.23	.21	.21	.24	.09	.07	.08	.09
Elongation	Sample Size	(-)	ND	ND	4	8	8	ND	ND	ND	ND	ND	6	6	5	6
	Mean	(mm)			+.42	+.26	+.24						+.23	+.14	+.50	-.04
	± RMS	(mm)			.13	.06	.48						.12	.26	.51	.21

NA ≡ Not applicable
ND ≡ Not determined
All data are preliminary
Fluences and temperatures are time and/or volume averages
Measurement errors Residual Bow ±0.07 mm (1σ)
Elongation ±0.12mm (1σ)

TABLE III SUMMARY OF PRESSURE BURST, RADIAL COMPRESSION AND IN-PLANE STRAIN MEASUREMENTS FOR 20 MM SLICES CUT FROM PEACH BOTTOM HTGR FUEL TEST ELEMENTS

H-327 TEST SPECIMENS			PRESSURE BURST TEST			RADIAL COMPRESSION TEST			IN-PLANE STRAIN MEASUREMENTS				
										GROOVE CHANGE		OUTER DIAM. CHANGE	
Element Type	Body ID	Graphite ID	Sample Size	Pressure ± 0.04 MPa (1σ) Mean	± RMS	Sample Size	Force ± 0.02 kN (1σ) Mean	± RMS	Sample Size	± 0.010 mm (1σ) Mean	± RMS	± 0.002 mm (1σ) Mean	± RMS
			(-)	(MPa)	(MPa)	(-)	(kN)	(kN)	(-)	(mm)	(mm)	(mm)	(mm)
UNIRRADIATED CONTROL TESTS													
6 Hole	1	1390	69	3.41	0.39	9	1.35	0.16	3	-0.004	0.003	-0.007	0.006
	2	1390	65	3.00	0.42	9	1.34	0.11	3	+0.025	0.004	-0.003	0.001
	3	1390	138	3.33	0.38	21	1.32	0.13	7	-0.004	0.011	-0.002	0.003
	4	1390	163	3.22	0.48	22	1.45	0.12	7	-0.009	0.006	-0.003	0.004
	Mean		435	3.25	0.44	61	1.38	0.14	20	-0.001	0.014	-0.004	0.004
8 Hole	6	1390	98	3.57	0.33	7	0.50	0.02	3	-0.025	0.026	-0.001	0.001
	7	1390	102	3.09	0.38	7	0.46	0.01	3	+0.029	0.013	-0.003	0.005
	8	1390	223	3.15	0.46	17	0.49	0.04	7	+0.011	0.014	-0.003	0.002
	Mean		423	3.23	0.45	31	0.49	0.03	13	+0.007	0.026	-0.003	0.003
8 Hole	RTE-3X2	2270	54	2.45	0.34	0	NA	NA	0				
8 Hole	RTE-ORNL	<1000	73	3.32	0.39	10	0.50	0.01	0				
8 HOLE TELEDIAL IRR. TEST													
FTE-1	2	2190	110	2.37	0.45	7	0.46	0.08	7	-0.207	0.073	-0.052	0.013
FTE-3	1	2150	83	2.97	0.35	9	0.42	0.03	6	-0.305	0.068	-0.053	0.018
	2	2270	23	3.11	0.25	1	0.44	0	2	-0.262	0.013	-0.048	0.005
	3	1830	67	2.08	.30	7	0.37	0.04	5	-0.240	0.030	-0.044	0.010
	Mean		173	2.64	0.55	17	0.40	0.04	13	-0.273	0.059	-0.049	0.014
FTE-4	1	1880	142	2.71	0.45	9	0.47	0.04	9	-0.207	0.065	-0.056	0.040
	2	1830	30	2.27	0.22	5	0.44	0.08	2	-0.309	0.024	-0.062	0.001
	3	1830	142	2.31	0.40	11	0.41	0.04	10	-0.213	0.058	-0.038	0.014
	Mean		314	2.49	0.46	25	0.44	0.06	21	-0.219	0.066	-0.048	0.030
6 HOLE TELEDIAL IRR. TEST													
FTE-14	1	2040	98	3.91	0.62	9	1.75	0.12	9	-0.150	0.050	-0.028	0.014
	2	2040	27	4.36	0.49	3	2.22	0.54	3	-0.207	0.018	-0.038	0.011
	3	2590	109	3.71	0.63	11	1.80	0.33	11	-0.148	0.034	-0.029	0.010
	Mean		234	3.87	0.64	23	1.84	0.34	23	-0.157	0.044	-0.030	0.012
FTE-15	1	2015	18	4.63	0.31	3	1.79	0.16	N.D.				
	2	2040	5	5.43	0.42	2	2.00	<0.01	N.D.				
	3	2040	18	3.91	0.89	3	1.70	0.22	N.D.				
	Mean		41	4.41	0.82	8	1.81	0.20	N.D.				
OUTER RING TEST													
UNIRRAD	6,7,8	1390				9	0.17	0.01					
FTE-3	3	1830				1	0.19	0					
FTE-4	1,2,3	1880/1830				3	0.25	<0.01					

All data are preliminary

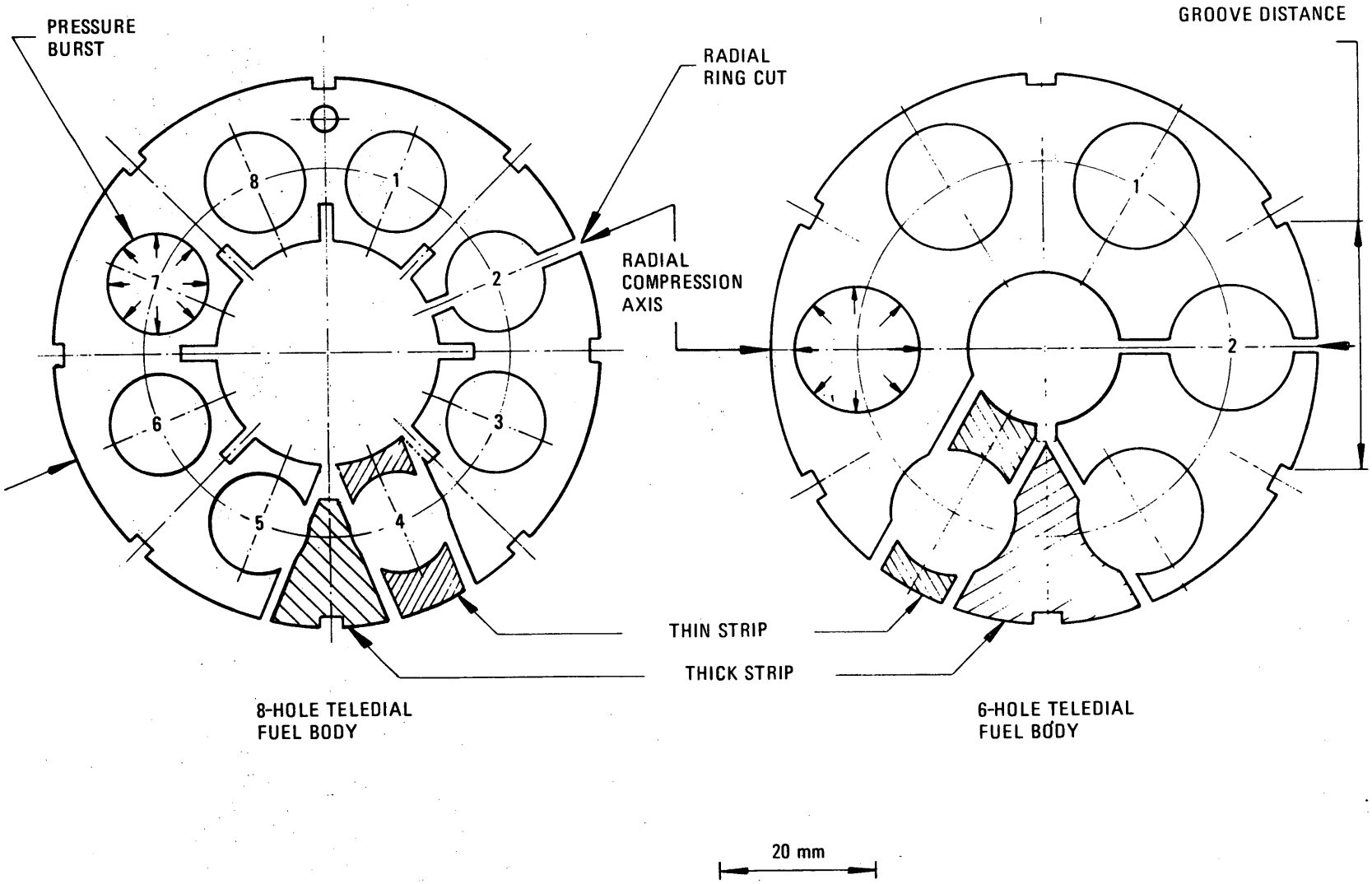

Fig. 1. Cross sections of Peach Bottom teledial fuel test elements

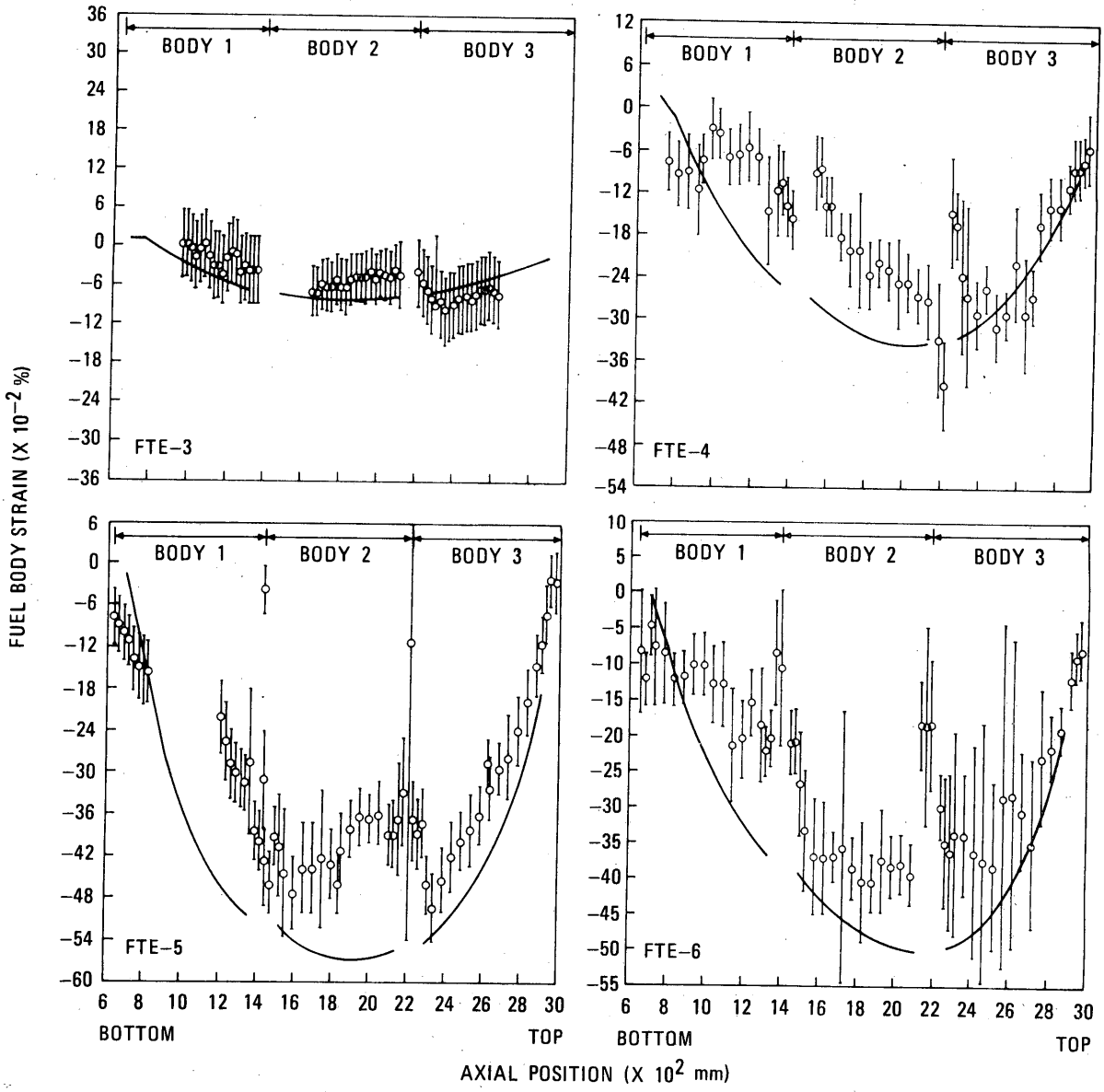

Fig. 2. Diametrical strain measurements (mean ± 2σ) and predictions for four eight-hole teledial elements irradiated in the Peach Bottom HTGR

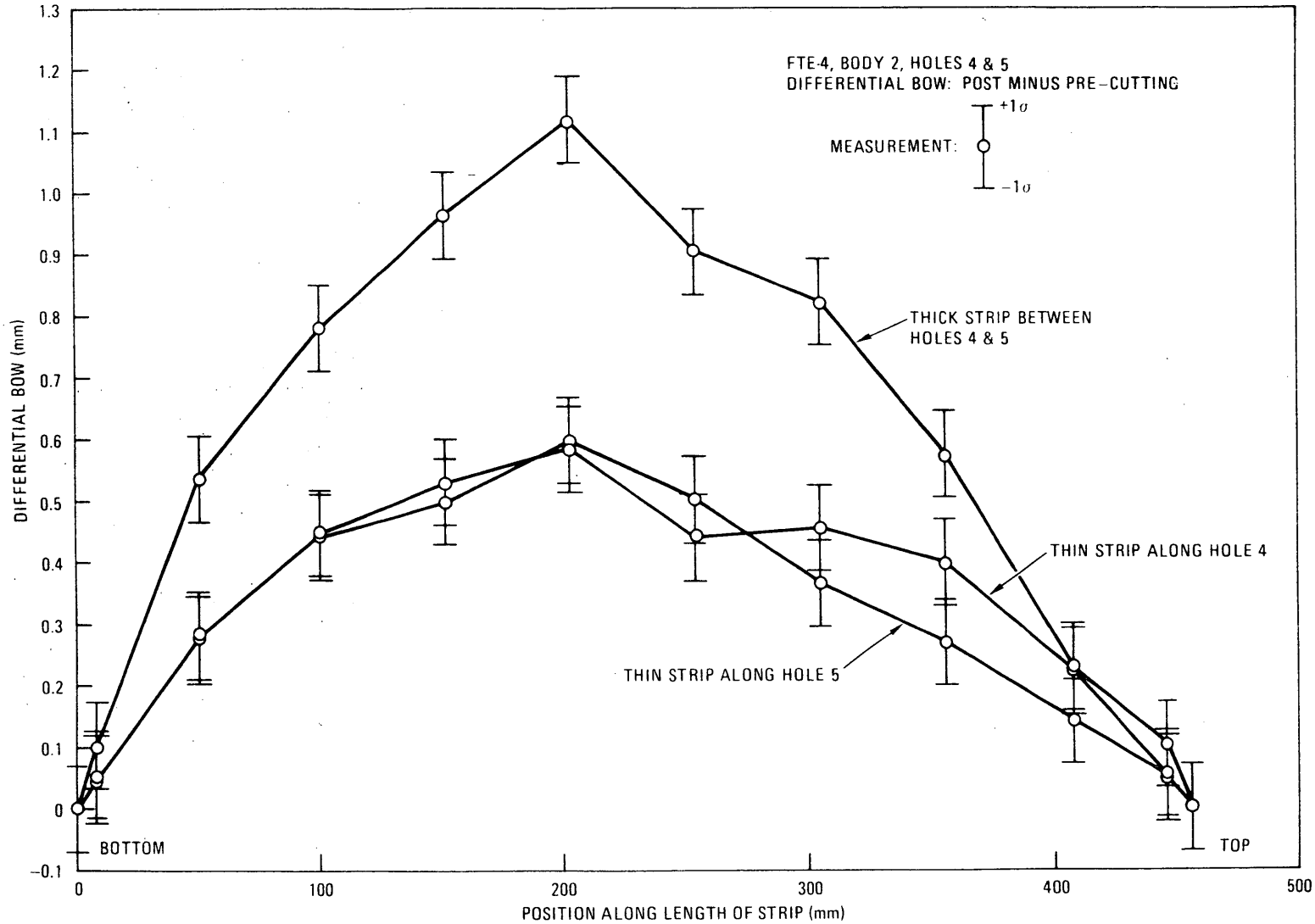

Fig. 3. Typical residual bow line determined for one thick strip and two adjacent thin strips

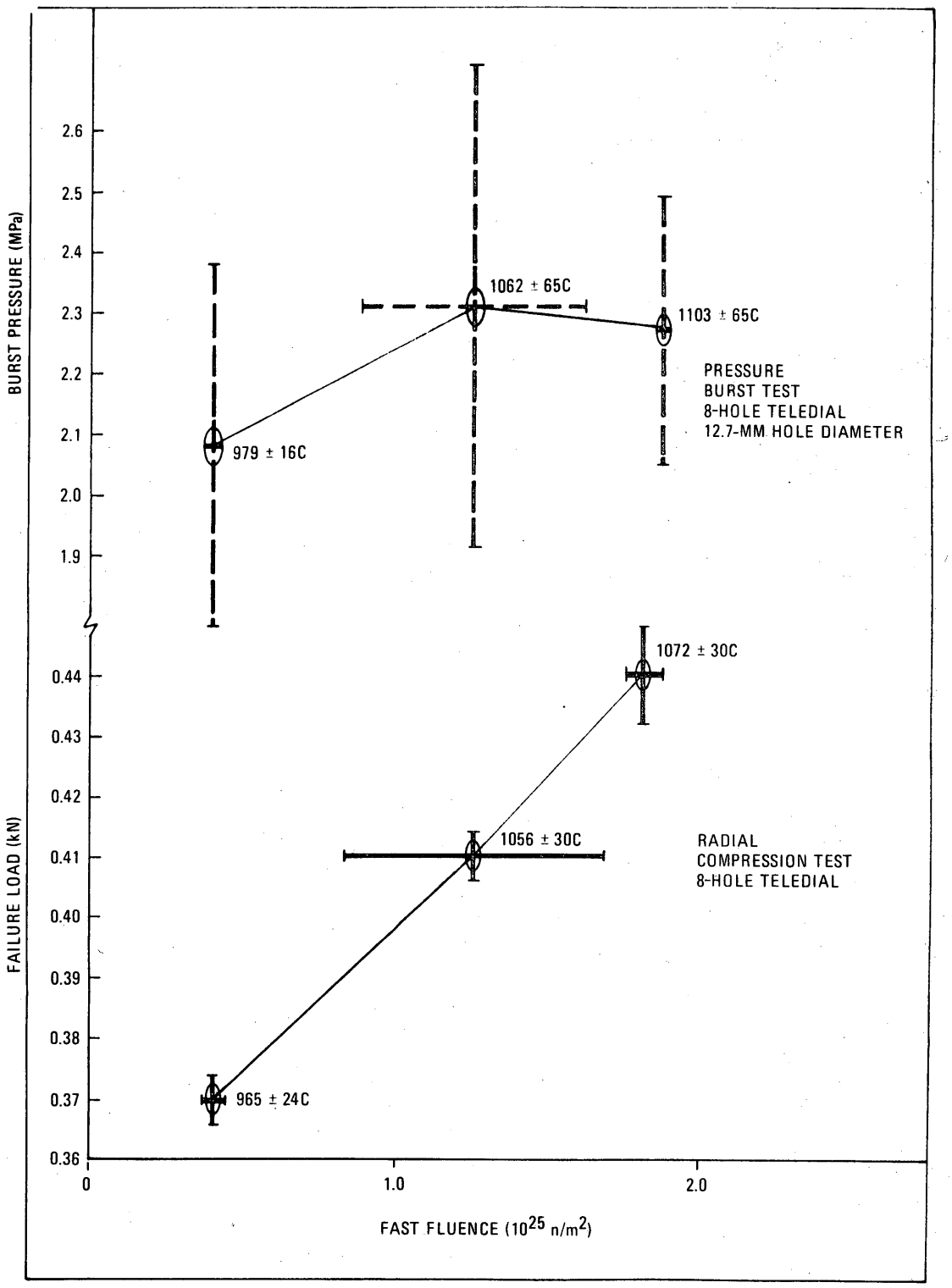

Fig. 4. Primary load test results versus fast fluence for eight-hole teledial slices

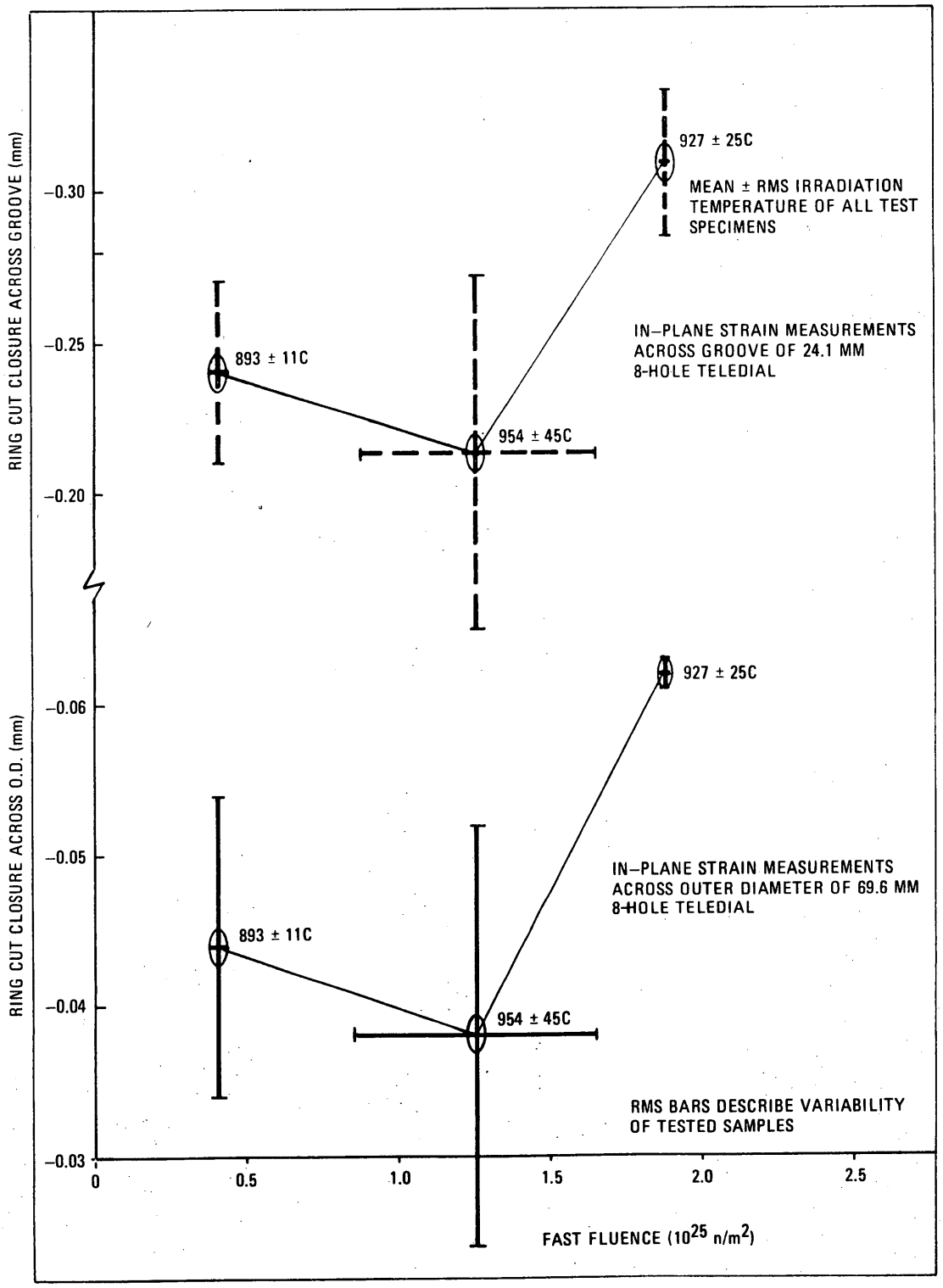

Fig. 5. In-plane strain measurements versus fast fluence for eight-hole teledial slices

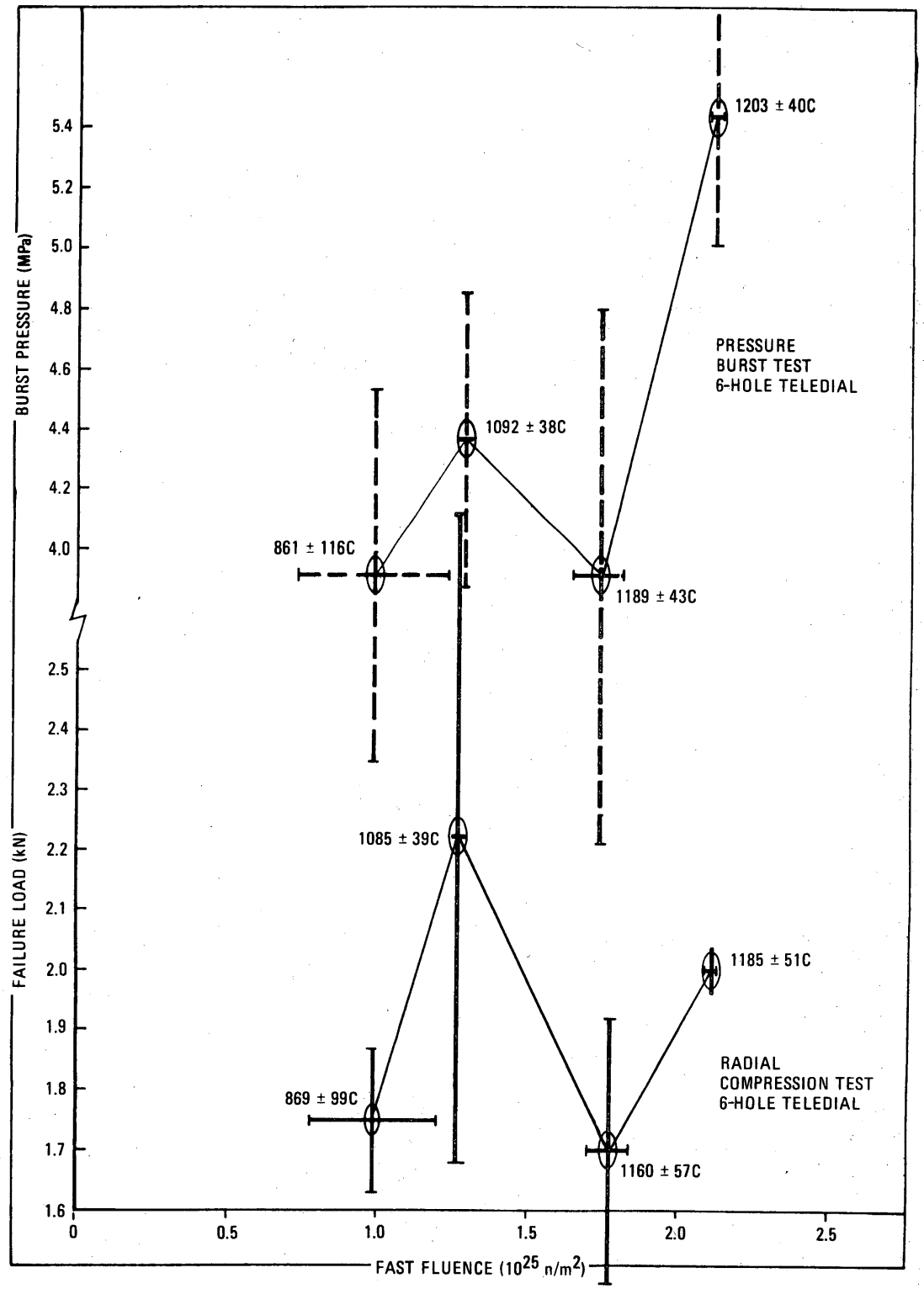

Fig. 6. Primary load test results versus fast fluence for six-hole teledial slices

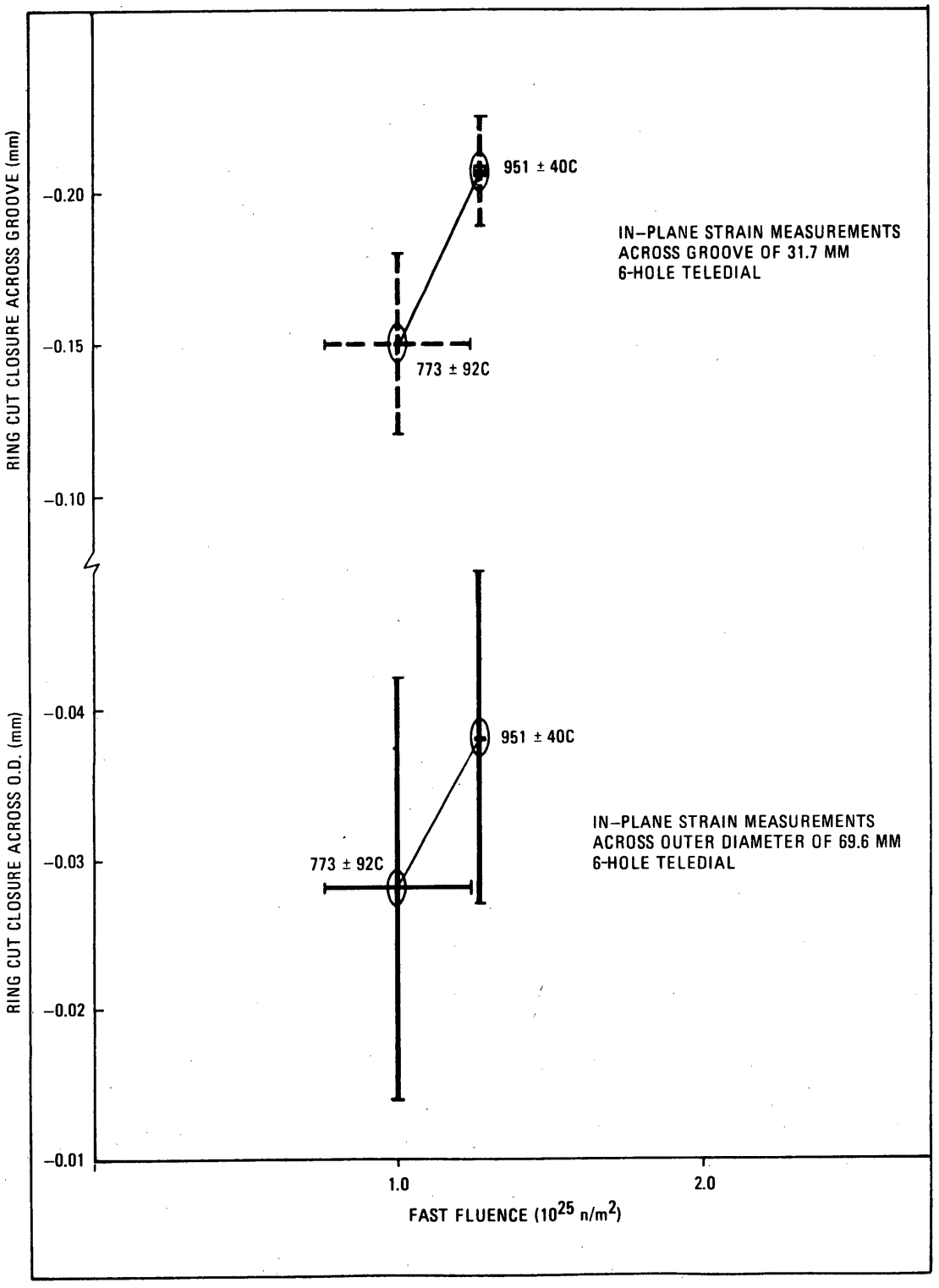

Fig. 7. In-plane strain measurements versus fast fluence for six-hole teledial slices